Influence of SiC technology in a Railway Traction DC-DC Converter Design Evolution

Alejandro Rujas, Víctor M. López, Asier García-Bediaga
Power Electronics Area
IK4-IKERLAN Technological Research Centre
20500 Arrasate-Mondragón, Spain
Email: arujas@ikerlan.es

Aloña Berasategi, Txomin Nieva
CAF Power & Automation
20271 Irura, Spain

***Abstract*—The introduction in the semiconductor market of the SiC technology enables power designers the development of power converters with higher power density (W/m^3) in comparison with the traditional converters based on Si power semiconductors. This work presents the redesign of a DC-DC converter, used in railway traction applications with full-SiC modules. The low current rating of the actual full-SiC modules makes necessary the use of several modules to substitute the "traditional" Si ones. This is considered in this work, together with the phase inductor design with amorphous magnetic materials, suitable for high current and high frequency levels. A comparison in terms of switching frequency, volume, magnetic elements and cooling system size, etc, is done, with the improvement possibilities offered by the introduction of this SiC technology.**

As result, the first DC-DC full-SiC converter for railway application is presented, as interface between the DC-link catenary and the energy storage system (ESS).

***Index Terms*—Silicon Carbide (SiC), DC-DC power converters, energy storage, supercapacitors.**

I. Introduction

As it is well-known, the evolution of power converters tends to develop higher efficiency and power density conversion systems. These goals are being carried out thanks to advanced converter topologies, as well as new power semiconductor devices with better static and dynamic features [1], [2].

From the point of view of the power devices, the interest of Wide Band Gap (WBG) semiconductors has considerable increased. Silicon Carbide (SiC) and Gallium Nitride (GaN) are the most promising materials because of their beneficial properties [1].

Talking about the market, the availability of SiC power modules is still limited. Traction systems normally use power modules with blocking voltage levels from 1,7kV to 6,5kV. The market started offering SiC Hybrid power modules (composed by a Silicon IGBT and a SiC freewheeling diode). Afterwards, samples of full-SiC devices (SiC MOSFET and diode) can be obtained. Therefore, recent works have presented new designs with SiC modules, like [3], where the complete design of a voltage source inverter with 1200 V/100 A full-SiC modules is presented, considering the switching characteristics, thermal analysis and gate driver and busbar design. In the same way, in [4] a discrete half bridge 1700 V/480 A SiC power block is presented with the same design concepts, depicting in detail the DC busbar design with low stray inductance and the air cooled heatsink results.

The parallel connection of five SiC MOSFET modules is covered in [5], with a design of a 312-kVA 3-phase inverter where the DC-link capacitor is made up by a network of distributed capacitors with the aim of decreasing the stray inductance, and also in [6] for 1200 V/ 100 A modules, with the same considerations.

SiC devices show also different considerations in terms of the gate driver design, therefore works like [7] present new design considerations for the gate driver circuitry.

The impact of the SiC MOSFET modules in the automotive industry for Hybrid and Plug-In Hybrid Electric Vehicles, is presented in [8], [9], where the efficiency is an important figure of merit.

This work presents the performances given by the SiC technology evolution in a 750 V DC-DC converter used in railway traction applications as interface between traction inverter, the catenary, and an energy storage system [10], [11]. A block diagram with the overall system description is presented in Fig. 1. A traction machine (M) is supplied by a traction inverter, connected to the DC-link with an input filter. And from the DC-link, via an input filter and a DC-DC converter, a energy storage system is used as auxiliary supply energy system. The DC-link is connected to a 750 V catenary with a circuit breaker. The modifications and improvements achieved in the DC-DC converter with the introduction of the SiC technology (highlighted in yellow) are presented in this paper.

A picture of the original whole Si-based system is presented in Fig. 2, where the DC-DC converter is highlighted in yellow. This system is used in railway traction applications as interface with an energy storage system, such as ultraca-

978-1-5090-2998-3/17/$31.00 ©2017 IEEE

Authorized licensed use limited to: b-on: UNIVERSIDADE DO PORTO. Downloaded on November 14,2022 at 14:30:43 UTC from IEEE Xplore. Restrictions apply.

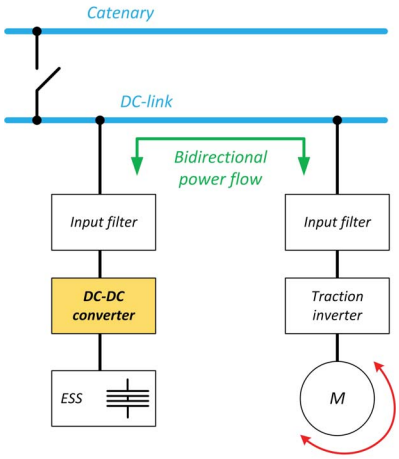

Fig. 1: Total system block diagram.

Fig. 2: Whole system converter, with the traction inverter and the DC-DC converter.

pacitors or batteries, as is presented in [11] for the company CAF Power & Automotion, as the first version of the ACR Evodrive/Freedrive [12], presented in Fig. 3 where the tram is able to operate without catenary. A scheme of the original Si version of the DC-DC converter is presented in Figure 4. It is made-up by four interleaved legs, and all the outputs are connected to the Energy Storage System (ESS). The ESS takes the energy of the whole system under the breaking conditions. The Si-based prototype is developed with the FF1000R17E4 IGBT modules from Infineon (1700V / 1000 A) commented previously, and the new Full-SiC prototype is designed with the Wolfspeed CAS300M17BM2 modules.

In this work, first, the modules offered by the market are enumerated, both for SiC hybrid and full-SiC solutions. Also the characteristics of a Full-SiC module with a typical Si-one are presented, considering the parallelization of modules.

Section III deals with the interleaved DC-DC converter design, paying special attention in the inductors design using amorphous magnetic materials. The papers ends with the

Fig. 3: Tram without catenary, working with the ACR-Freedrive.

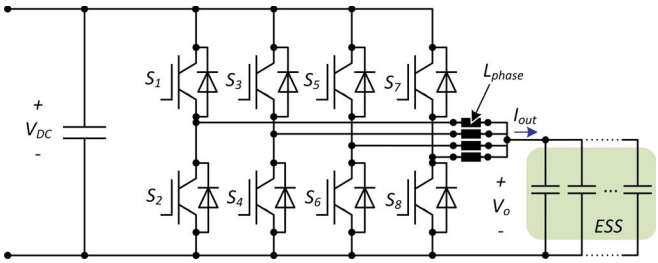

Fig. 4: DC/DC converter under study.

presentation of some experimental results and the conclusions achieved.

II. Full-SiC vs. Si devices

The SiC power devices are divided in two types: Full-SiC modules and Hybrid-SiC modules, as it has been commented previously. The available SiC hybrid power modules that can be used in traction systems are listed in the Table I, and the full-SiC ones are presented in Table II.

The power semiconductors market is changing introducing and offering new SiC devices. The introduction of the SiC

TABLE I: Available SiC Hybrid Modules.

Manufacturer	Reference	Voltage	Current	Packaging (mm x mm)
Infineon	**FF1000R17IE4F**	**1700 V**	**1000 A**	**250 x 90**
Mitsubishi	CMH1200DC-34S	1700 V	1200 A	140 x 130
Fuji	2MSi 1200VAT-170EC	1700 V	1200 A	140 x 130
Hitachi	MBM450FS33F-C	3300 V	450 A	100 x 140

TABLE II: Available Full-SiC Modules.

Manufacturer	Reference	Voltage	Current	Packaging (mm x mm)
Wolfspeed/Cree	CAS300M12BM2	1200 V	300 A	62 x 106
Mitsubishi	FMF800DX-24A	1200 V	800 A	62 x 122
Mitsubishi	FMF1200DX1-24A	1200 V	1200 A	122 x 122
Wolfspeed/Cree	**CAS300M17BM2**	**1700 V**	**225 A**	**62 x 106**
Semikron	SKM260MB170SCH17	1700 V	385 A	62 x 106

Authorized licensed use limited to: b-on: UNIVERSIDADE DO PORTO. Downloaded on November 14,2022 at 14:30:43 UTC from IEEE Xplore. Restrictions apply.

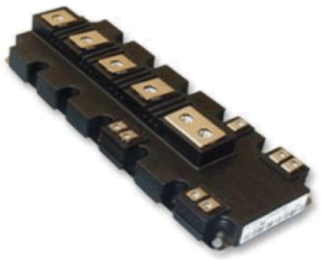

Fig. 5: Si power module.

Fig. 6: Full-SiC power module.

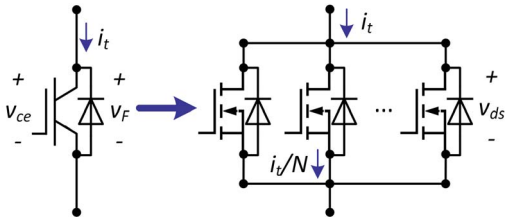

Fig. 7: Parallelization of SiC switches.

technology makes possible higher switching frequencies, with higher di/dt values in the switching transitions. With the aim of driving higher current ratings with SiC devices, the manufacturers are offering new packaging solutions with low overall stray inductance [13], [14], that are gaining interest in the market, named LinPak by ABB, XHP by Infineon, or nHPD2 by Hitachi. Due to that, new Hybrid and Si-based devices with voltage/current rates of 3300 V/450 A and 1700 V/900 A are offered, trying to represent a stepforward compared with the "traditional" power semiconductor packages (PrimePack or IHV from Infineon, HiPak from ABB, etc). The modularity and easy paralleling is also an important advantage offered by the new packaging solution, that according to [15] reduces the internal inductance by 75 % from the conventional modules. In parallel, new Full-SiC modules are offered, but without the high current levels mentioned before. Due to that, 62 mm package is the first module available for 1k7V voltages, with a 225A current rate.

In order to manage the same current level, it is necessary to connect full-SiC modules in parallel. With the aim of making a real comparison, hereafter it is presented the conduction and switching characteristics of the FF1000R17E4 Si-based module (Primepack package, Fig. 5) from Infineon, and the CAS300M17BM2 (62 mm package, Fig. 6) module from Wolfspeed. Figure 7 represents the basic concept of switch parallelization. With this, the switching losses in the IGBT module are given by:

$$p_{cond,IGBT}(i_t) = v_{ce}(i_t) \times i_t \times d \tag{1}$$

$$p_{cond,D}(i_t) = v_F(i_t) \times i_t \times (1-d) \tag{2}$$

$$E_{sw}(i_t) = E_{on}(i_t) + E_{off}(i_t) + E_{rr}(i_t), \tag{3}$$

where $v_{ce}(i_t)$ and $v_F(i_t)$ represents IGBT and diode conduction voltage as function of the device current i_t, respectively. d represents the duty cycle, and $E_{on}(i_t)$, $E_{off}(i_t)$ and $E_{rr}(i_t)$ the switching energies, also function of the current. As result, the IGBT and diode conduction losses ($p_{cond,IGBT}$ and $p_{cond,D}$), and the total switching energy E_{sw} are obtained as function of i_t.

In the same way, the losses when N full-SiC devices are paralleled, are given by:

$$p_{cond,M}(i_t) = v_{ds}\left(\frac{i_t}{N}\right) \times i_t \times d \tag{4}$$

$$p_{cond,3^{er}}(i_t) = v_{3^{rd}}\left(\frac{i_t}{N}\right) \times i_t \times (1-d) \tag{5}$$

$$E_{sw}(i_t) = \left(E_{on}\left(\frac{i_t}{N}\right) + E_{off}\left(\frac{i_t}{N}\right) + E_{rr}\left(\frac{i_t}{N}\right)\right) \times N, \tag{6}$$

where $v_{ds}(i_t/N)$ and $v_{3^{rd}}(i_t/N)$ represents MOSFET conduction voltage in the 1^{st} and 3^{rd} quadrant, respectively, as function of the total current i_t and the number of module in parallel N.

For a better understanding of the modules comparison, the terms $v_{ce}(i_t) \times i_t$ and $v_{ds}(i_t/N) \times i_t$ for both modules are plotted together in Fig. 8. In the same way, the terms $v_F(i_t) \times i_t$ and $v_{3^{rd}}(i_t/N) \times i_t$ are plotted in Fig. 9. The Si results for the FF1000R17E4 are represented in the dash-dot line, and the SiC CAS300M17BM2 result for different modules in parallel are represented in solid lines.

It can be seen that the IGBT has a better conduction characteristic, and 4 SiC modules are needed to obtain a similar conduction behavior with a current lower than 450 A. However, the conduction behavior of the MOSFET in the 3^{rd} quadrant is quite better (Fig. 9), and the use of 2 SiC modules in parallel gives a similar conduction results than the freewheeling diode of the Si module. This is an important aspect that does not occur under the use of SiC Hybrid modules, where the SiC diode has a worse conduction characteristics than the Si one [16].

The switching energy E_{sw}, values are plotted in Fig. 10. As it is well-known, the switching performance of SiC devices is the stepforward that makes this technology attractive. It can be appreciated that the E_{sw} for the Full-SiC device is around 12 times lower than the Si-based device. Also, the total E_{sw} value is the same with different N modules in parallel due to

Authorized licensed use limited to: b-on: UNIVERSIDADE DO PORTO. Downloaded on November 14,2022 at 14:30:43 UTC from IEEE Xplore. Restrictions apply.

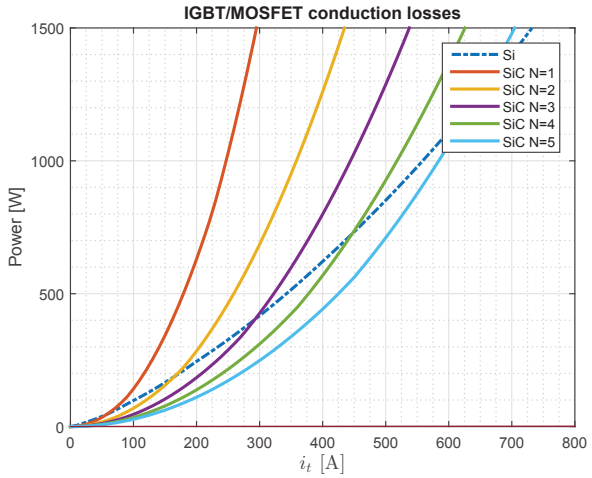

Fig. 8: $v_{ce}(i_t) \times i_t$ term comparison between FF1000R17E4 and CAS300M17BM2 device.

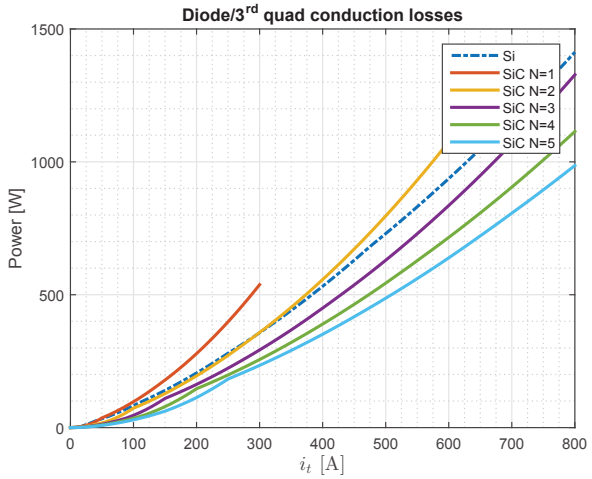

Fig. 9: $v_F(i_t) \times i_t$ term comparison between FF1000R17E4 and CAS300M17BM2 device.

the linear characteristic of E_{sw} with the current shown by the Wolfspeed module under study.

Another aspect to take into consideration is the size of the power modules. The size of the Si-based FF1000R17E4 is 89×234 mm (W×L), and 62×106 mm for the CAS300M17BM2 module. This yields with an area ratio per module of $A_{SiC}/A_{Si} = 31\%$. The size of the module affects also in the junction-to-case thermal resistance R_{thjc}, of the IGBT/MOSFET and the diode, whose values are listed hereafter:

- Si FF1000R17E4
  - $R_{thjc,IGBT} = 24°C/kW$
  - $R_{thjc,D} = 48°C/kW$
- Full-SiC CAS300M17BM2

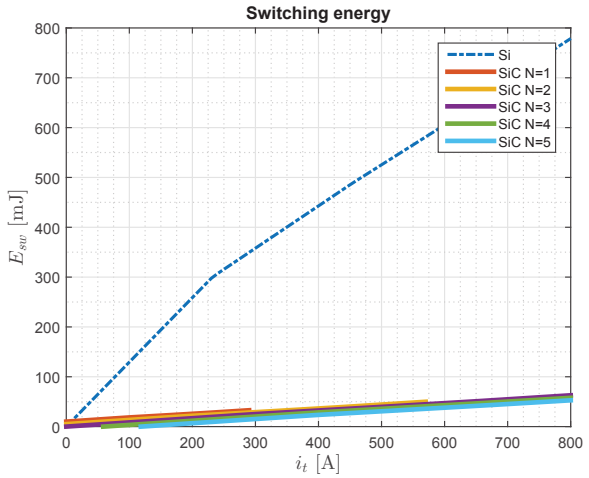

Fig. 10: E_{sw} term comparison between FF1000R17E4 and CAS300M17BM2 device.

  - $R_{thjc,M} = 67°C/kW$
  - $R_{thjc,D} = 60°C/kW$

As it is presented in [17], SiC has a better thermal conductivity than Si, therefore the SiC power devices needs lower chip area for having the same R_{thjc} values. This aspect corresponds with the values presented before for the modules under comparison, obtaining:

$$R_{thjc,SiC} < R_{thjc,Si} \times \frac{A_{Si}}{A_{SiC}}. \tag{7}$$

Although the switching losses improvement represents the main advantage of the SiC power modules, this thermal enhance must be also considered because represents the possibility of managing more losses in terms of W/mm^2 than the Si devices (i.e. the reduction of the power core).

III. Full-SiC DC-DC converter

The Si-based converter under study was introduced previously in Fig. 4. It is a high power DC/DC converter with the next specifications:

- Nominal input voltage (V_{dc}): 750 V.
- Maximum output voltage (V_o): 490 V.
- Nominal Power (P): 225 kW (470 kW peak).
- Maximum output current ($I_{o,max}$): 1750 A.
- Maximum ambient temperature (T_{amb}): 45 °C.

The switching frequency of the original DC-DC converter is 2 kHz. A previous work presents the SiC-Hybrid version [16], which is done with the FF1000R17IE4F, from Infineon also. The package dimensions of the Si and SiC-Hybrid modules are exactly the same, with the same current and voltage rates. Due to that, a direct substitution of the Si modules by the

Authorized licensed use limited to: b-on: UNIVERSIDADE DO PORTO. Downloaded on November 14,2022 at 14:30:43 UTC from IEEE Xplore. Restrictions apply.

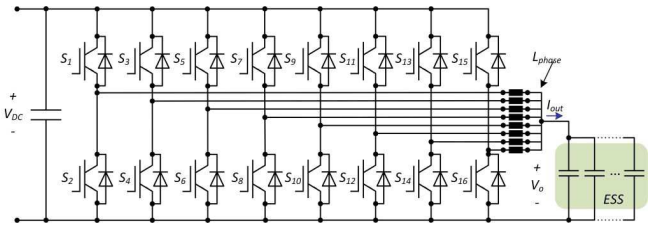

Fig. 11: Full-SiC converter scheme.

SiC-Hybrid ones is presented, obtaining a "hybrid" converter version which is able to operate at 6 kHz. Nevertheless, the huge differences with the full-SiC modules gives rise to the development of a totally new DC-DC design.

The SiC power module selected is 225A current rate [18]. It is still low current rated compared to the original Si one, so in this case a connection of several branches in parallel is needed.

The paralleling analysis done in Section II is the same for interleaved legs. Each leg of the converter is phase shifted $360/N_t$ degrees, being N_t the total number of interleaved legs (the paremeter N, introduced in Section II, represents the number of SiC modules in parallel/interleaving per each IGBT Si module). The duty cycle is given by $d = V_o/V_{dc}$, and defining $d' = 1 - d$, the current ripple is given by (8).

$$\Delta i_L = \frac{V_o}{2 f_{sw} L N_t} \times \\ \times \left[floor(d' N_t) + 1 - d' N_t \right] \left[d' N_t - floor(d' N_t) \right]. \quad (8)$$

The optimal design, in terms of volume, weight and efficiency, is determined by the selection of the proper switching frequency and the number of phases of the converter, following the design steps depicted in [19]. This design procedure leads in a eight interleaved legs ($N_t = 8$), with a switching frequency of 30 kHz. As result, the nominal current in each leg is 75 A, with a maximum value of 218 A. A scheme of the new 8-legs converter is shown in Fig. 11. The peak-to-peak current ripple is defined as 50 A_{pp} ($\Delta i_L = 25A$), corresponding with a phase inductance needed of $L = 150\mu H$. The maximum allowed dimensions for all the inductors are 565×240×90 mmm (W×L×D).

For the magnetic design, four different types of magnetic core materials have been considered, whose characteristics are presented in Table III:
- Ferrite core (N27).
- Powder core (Kool mμ).
- Nanocrystaline (VITROPERM).
- Amorphous core (2605SA1).

As it is well-known, under high-current designs, the most restrictive constraint is the core saturation (B_{max}). A complete inductor size calculation is done for the four different materials, considering also the relative permeability (μ_i), as it is presented hereafter.

TABLE III: MAGNETIC MATERIAL CHARACTERISTICS.

Material	B_{max}	μ_i
N27	350 mT	1800
Kool-mμ	800 mT	26-125
VITROPREM	1200 mT	5000
2605SA1	1500 mT	1000

For each material, the term $N_{turns} \times A_c$ is a constant value that can be written as:

$$N_{turns} \times A_c = \frac{L(I_L + \Delta i_L)}{B_{max}}, \quad (9)$$

being N_{turns} the number of turns, and A_c the core area. In addition, N_{turns} can be also written as function of the air gap (l_g), and the path core (l_m) as follows:

$$N_{turns} = \frac{B_{max} \left(l_g + \frac{l_m}{\mu_i} \right)}{\mu_o (I_L + \Delta i_L)}. \quad (10)$$

The total width (W) and length (L) are computed for different values of A_c and l_m. For these different values, the number of turns and the air gap can be calculated by (9) and (10), respectively. Fig. 12 shows the result of these calculation, where the total dimension constraints are highlighted in yellow.

It can be seen that N27 Ferrite cores do not fulfill the required dimensions, and using Kool-mμ cores is around the dimension limits. Nanocrystaline cores fit the dimensions, but represents a more expensive solution, due to that 2605SA1 amorphous core is selected. Despite of the magnetostriction noise effect typical of the amorphous core materials, the high switching frequency selected in this application does not cause this noise effect.

Among the different available amorphous cores, the AMCC32 is selected, from Metglas, with a core area (A_c) of 3.2 cm^2, with a dimensions of 30×41×82 mm, and a path length $l_m = 20$ cm. Each phase inductor is composed by 6 AMCC32 cores (3 rows × 2 columns of cores). With these parameters it is possible to calculate the number of turns N_{turns}, and the air gap l_g, given by (11) and (12), respectively. The inductors were manufactured as it is presented in Fig. 13.

$$N_{turns} = \frac{L(I_L + \Delta i_L)}{A_c B_{max} 0.9} = \frac{150\mu H \times (218 + 25A)}{6 \times 3.2 cm^2 \times 1500 mT} \approx 13, \quad (11)$$

$$l_g = \frac{\mu_0 N_{turns} (I_L + \Delta i_L)}{B_{max}} - \frac{l_m}{\mu_i} = \\ = \frac{4\pi 10^{-7} \times 13 \times (218 + 25A)}{1500 mT} - \frac{20cm}{1000} \approx 4mm, \quad (12)$$

Thus, a complete simulation is done obtaining a power losses

Authorized licensed use limited to: b-on: UNIVERSIDADE DO PORTO. Downloaded on November 14,2022 at 14:30:43 UTC from IEEE Xplore. Restrictions apply.

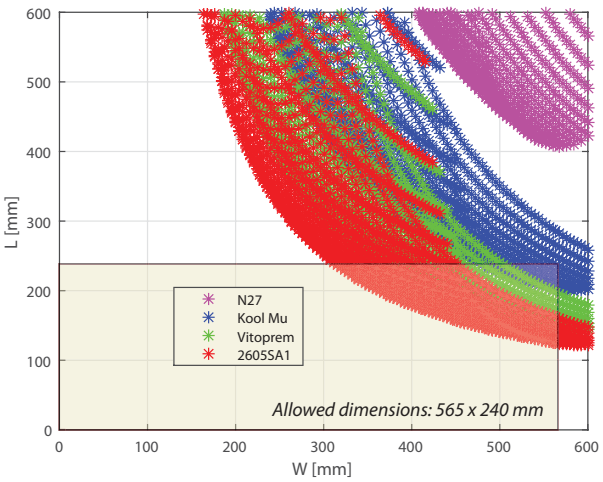

Fig. 12: Inductors size for different materials. In yellow, it is highlighted the maximum allowed dimensions.

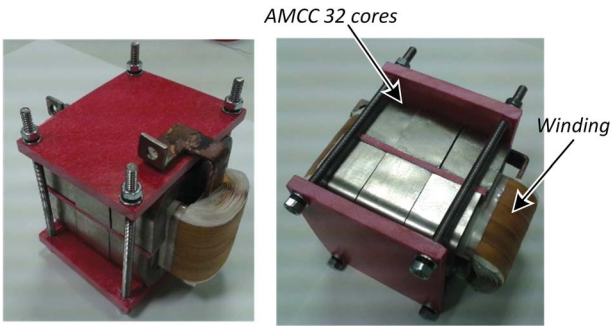

Fig. 13: Inductors developed for the prototype.

reduction in the full-SiC converter of the 30 % at nominal power (225 kW), and around a 50 % of losses reduction at 150 kW, despite of the increment in the switching frequency. This important power losses reduction, and the redesign using full-SiC modules enables an important reduction in the size of the whole converter. The main reductions are in the power core (i.e. the heatsink), and in the phase inductors.

The reduction of the phase inductors is shown in Fig. 14. The volume of the new eight inductors is 73 % lower than the inductors of the Si-based original converter, improving the size of the overall system. The reduction in the power core size is illustrated in Fig. 15, where the size reduction is the 40 % in comparison with the original version. With this, the size of the whole system decreases, being totally new. This aspect is presented in Fig. 16, with a total volume reduction of the 30 % in comparison with the initial Si design.

IV. Experimental Results

The DC-DC converter has been developed according to the presented electromechanical design, and tested at different

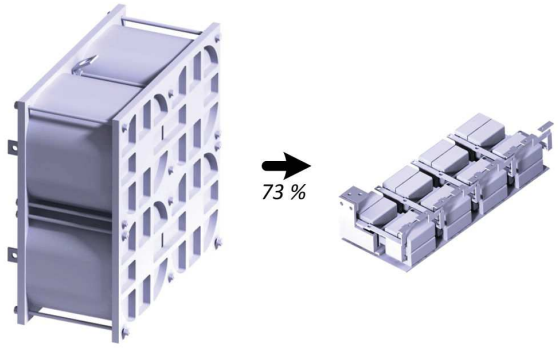

Fig. 14: Comparison of the phase inductor size. Left: Old inductor phases. Right: New inductors.

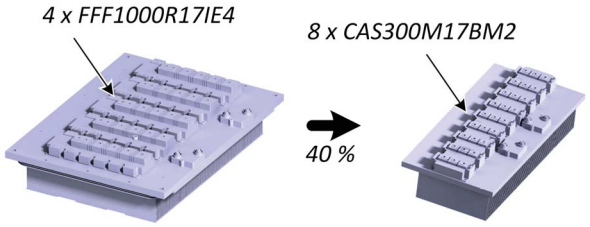

Fig. 15: Comparison of the power core size. Left: Si power core. Right: Full-SiC version.

power levels. A picture of the power core with the gate drivers and the DC-link capacitor, and the power inductors is presented in Fig. 17, where it can be appreciated the placement of the main contactor over the phase inductors. For a better understanding of the size reduction, the Full-SiC converter has been placed inside of the original converter envelope that was presented before in Fig 2. The reduction is highlighted with a red square in Fig. 18, corresponding with the 30 % commented previously.

The first experimental test corresponds with the behavior of the new inductors under different current levels. As it has been presented before, each inductor is made up by 6 AMCC32 amorphous magnetic cores, and it is designed to manage up

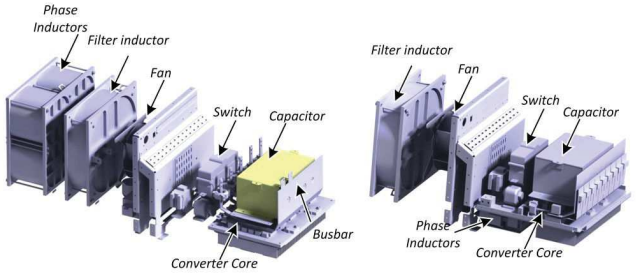

Fig. 16: Electromechanical design. Left: Original Si design. Right: Full-SiC converter design.

Authorized licensed use limited to: b-on: UNIVERSIDADE DO PORTO. Downloaded on November 14,2022 at 14:30:43 UTC from IEEE Xplore. Restrictions apply.

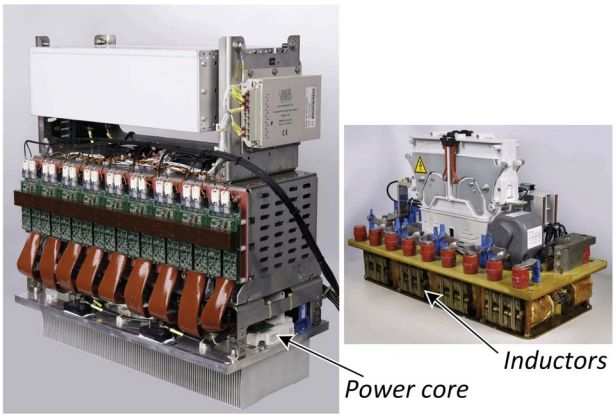

Fig. 17: Full-SiC Converter. Left: Power core with capactior and gate drivers. Right: power inductors and main contactor.

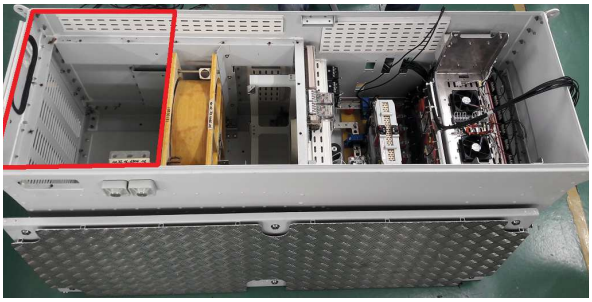

Fig. 18: New Full-SiC converter inside the original converter envelope.

to 245 A. The experimental measurements of the inductance values are presented in Fig. 19. The inductor values are calculated from the current ripple (Δi) measurements around the different average DC current levels. It can be appreciated how the inductance value L is around 170 μH, decreasing deeply with values higher than 250 A. This is confirmed for the eight inductances of the interleaved converter. The difference between the measured (170 μH) and the design value (150 μH) corresponds with an error of 13 %, due to the inductance tolerance.

The current ripple and the phase shift between the different converter legs is shown in Fig. 20 with an output current $I_{out} = 400$ A, that corresponds with the maximum available in the laboratory equipment. The current ripple is the same in the four sampled legs, $\Delta i_L = 10$ A (20 A_{pp}), with the correct phase shift between them, 45 deg.

The measured efficiency of the DC-DC converter is presented in Fig. 21 under different current and input/output voltage conditions, considering also the bidirectional behavior (as boost converter and as buck converter).

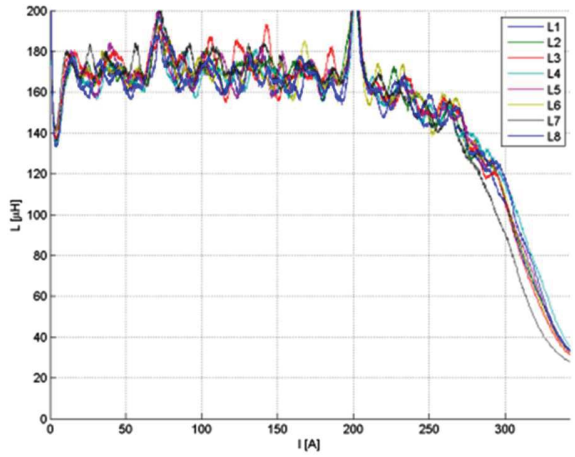

Fig. 19: Inductance value under different current levels.

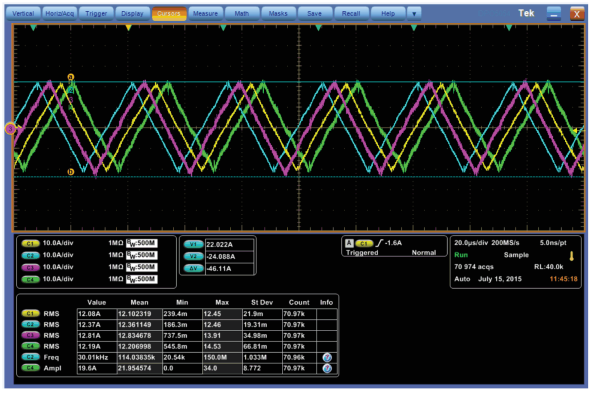

Fig. 20: Phase current waveforms in steady state.

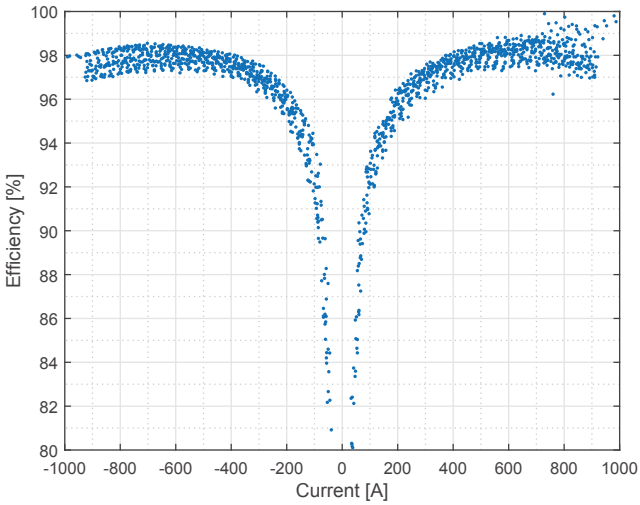

Fig. 21: DC-DC converter Efficiency under different current levels.

Authorized licensed use limited to: b-on: UNIVERSIDADE DO PORTO. Downloaded on November 14,2022 at 14:30:43 UTC from IEEE Xplore. Restrictions apply.

V. Conclusions

The influence of new power devices SiC technology in a real high power DC/DC converter used in railway applications is presented. The SiC-based technology power modules suitable for railways applications are still few. However, there are already some power devices in the market that can be used and studied. Full SiC devices with SiC MOSFET and SiC diode are used. The totally different packaging and current rate offered by the manufacturers makes necessary a complete redesign of the converter. A new full-SiC converter version is presented, with a total size reduction of the 30 % (with a 73% in the inductances, and a 40 % reduction in the heatsink).

First, a study has been done to find an optimal amount of modules connected in parallel to reach the suitable current levels. This study shows that replacing the original Si modules for Full-SiC modules, reduction in losses, size and weight are achieved. This implies a disminution of the cooling system and also of the magnetic elements in a complete redesign of the converter.

The low current rate of the full-SiC modules offered by the semiconductor manufacturers makes needed the design of the converter with several full-SiC modules in parallel or interleaved. Despite of that, the switching energy minimization enables a reduction of the power losses in spite of increasing the switching frequency more than 10 times the original value. As a result, the converter power core is a 40 % smaller than the Si-based one.

A new inductors design with amorphous magnetic cores is also presented, suitable for high current and high frequency levels, with also an important reduction of the inductors size, a 73 %. The reduction of the power core and inductors have been traduced to a 30% reductin of the total volume of the converter box.

Finally, the experimental results confirm the correct behavior of the whole system in terms of: correct current sharing and ripple in the interleaved phase legs, heat-sink temperatures evolution, and inductor desing under different current levels.

As result, the first Full-SiC DC-DC converter for railway applications is presented.

Acknowledgment

This project has received funding from the European Unions Horizon 2020 research and innovation programme under grant agreement No. 636032.

References

[1] J. Millan, P. Godignon, X. Perpina, A. Perez-Tomas, and J. Rebollo, "A Survey of Wide Bandgap Power Semiconductor Devices," *IEEE Transactions on Power Electronics*, vol. 29, no. 5, pp. 2155–2163, may 2014.

[2] A. Mantooth, "Devices and Components for New Power Converter Developments," *IEEE Power Electronics Magazine*, no. 6, pp. 53–56, June 2016.

[3] S. Hazra, S. Madhusoodhanan, G. K. Moghaddam, K. Hatua, and S. Bhattacharya, "Design Considerations and Performance Evaluation of 1200-V 100-A SiC MOSFET-Based Two-Level Voltage Source Converter," *IEEE Transactions on Industry Applications*, vol. 52, no. 5, pp. 4257–4268, sep 2016.

[4] X. She, R. Datta, M. Harfman-Todorovic, G. Mandrusiak, J. Dai, T. Frangieh, P. Cioffi, B. Rowden, and F. Mueller, "High Performance Silicon Carbide Power Block for Industry Applications," *IEEE Transactions on Industry Applications*, pp. 1–1, 2017.

[5] J. Colmenares, D. Peftitsis, J. Rabkowski, D.-P. Sadik, G. Tolstoy, and H.-P. Nee, "High-Efficiency 312-kVA Three-Phase Inverter Using Parallel Connection of Silicon Carbide MOSFET Power Modules," *IEEE Transactions on Industry Applications*, vol. 51, no. 6, pp. 4664–4676, nov 2015.

[6] J. Fabre and P. Ladoux, "Parallel Connection of 1200 V/100 A SiC MOSFET Half-bridge Modules," *IEEE Transactions on Industry Applications*, pp. 1–1, 2015.

[7] P. Anthony, N. McNeill, and D. Holliday, "High-Speed Resonant Gate Driver With Controlled Peak Gate Voltage for Silicon Carbide MOSFETs," *IEEE Transactions on Industry Applications*, vol. 50, no. 1, pp. 573–583, jan 2014.

[8] H. Zhang, L. M. Tolbert, and B. Ozpineci, "Impact of SiC Devices on Hybrid Electric and Plug-In Hybrid Electric Vehicles," *IEEE Transactions on Industry Applications*, vol. 47, no. 2, pp. 912–921, mar 2011.

[9] D. Han and B. Sarlioglu, "Comprehensive Study of the Performance of SiC MOSFET-Based Automotive DC?DC Converter Under the Influence of Parasitic Inductance," *IEEE Transactions on Industry Applications*, vol. 52, no. 6, pp. 5100–5111, nov 2016.

[10] L. Mir, H. G. naga, A. L. de Heredia, C. Calleja, and I. Etxeberria-Otadui, "Supercapacitor-based ride-through system for a 10 kw drive application," in *The XIX International Conference on Electrical Machines - ICEM 2010*, Sept 2010, pp. 1–6.

[11] L. Mir, I. Etxeberria-Otadui, I. P. de Arenaza, I. Sarasola, and T. Nieva, "A supercapacitor based light rail vehicle: system design and operations modes," in *2009 IEEE Energy Conversion Congress and Exposition*, Sept 2009, pp. 1632–1639.

[12] G. Abad, Ed., *Power Electronics and Electric Drives for Traction Applications*. Chichester, UK: John Wiley & Sons, Ltd, oct 2016. [Online]. Available: http://doi.wiley.com/10.1002/9781118954454

[13] R. Schnell, S. Hartmann, D. Trüssel, F. Fischer, A. Baschnagel, and M. Rahimo, "LinPak, a new low inductive phase-leg IGBT module with easy paralleling for high power density converter designs."

[14] R. Schnell, S. Hartmann, S. Kicin, and F. Fischer, "LinPak, the new standard expands to 3,300 V and shows excellent parallel operation as well as SiC readiness."

[15] D. Kawase, M. Inaba, K. Horiuchi, and K. Saito, "High voltage module with low internal inductance for next chip generation -next High Power Density Dual (nHPD2)." [Online]. Available: http://www.hitachi-power-semiconductor-device.co.jp/en/product/igbt/pdf/pcim_nHPD2.pdf

[16] J. San-Sebastian, A. Rujas, L. Mir, A. Berasategi, and T. Nieva, "Performance improvements using silicon carbide hybrid igbt modules in traction application," in *2016 International Conference on Electrical Systems for Aircraft, Railway, Ship Propulsion and Road Vehicles International Transportation Electrification Conference (ESARS-ITEC)*, Nov 2016, pp. 1–6.

[17] B. Ozpinecil, L. Tolbert, and S. Islam, "Silicon carbide power device characterization for HEVs," in *Power Electronics in Transportation, 2002*. IEEE, pp. 93–97.

[18] CREE, "CAS300M17BM2 Datasheet," 2014.

[19] A. Rujas, I. Villar, I. Etxeberria-Otadui, U. Larranaga, and T. Nieva, "Design and experimental validation of a silicon carbide 100kW battery charger operating at 60kHz," in *2014 IEEE 15th Workshop on Control and Modeling for Power Electronics (COMPEL)*. IEEE, jun 2014, pp. 1–7.

Authorized licensed use limited to: b-on: UNIVERSIDADE DO PORTO. Downloaded on November 14,2022 at 14:30:43 UTC from IEEE Xplore. Restrictions apply.